PLEASE CITE THIS ARTICLE AS DOI: 10.1063/5.0259927

Modelling the impact of drug-nanocarriers in lipid membranes

Germán Pérez-Sánchez,[a,*] João A. P. Coutinho[a] and Manuel Melle-Franco[a]

[a]CICECO – Aveiro Institute of Materials, Department of Chemistry, University of Aveiro, 3810-1933 - Aveiro, Portugal

[*]Corresponding author:

Dr. Germán Pérez-Sánchez

Researcher at CICECO – Aveiro Institute of Materials, University of Aveiro

gperez@ua.pt

Abstract

A coarse-grain framework for molecular dynamics (CG-MD) simulations based in the MARTINI force field was developed to tackle interactions between ionic G5 dendrimers and nonionic Pluronic micelles with diverse amphiphilic characters as drug-loaded nanocarriers in contact with two biological membranes, the anionic 1-palmitoyl-2-oleoyl-glycero-3-phosphocholine POPC + 1-palmitoyl-2-oleoyl POPG and the neutral dipalmitoyl phosphatidylcholine. Simulations showed that drug-nanocarrier stability relies on a delicate balance of their amphiphilic character and coulombic interactions. Pluronic micelles yielded lower undesired drug leaks into the water phase compared with the cationic G5 dendrimers, which either remained attached to Pluronic moieties or between them and the membrane surface. An interesting feature of Pluronic micelles was their tendency to be disrupted and absorbed into the membranes. Hydrophilic micelles showed improved drug stability, avoiding doxorubicin and gemcitabine early drug release. When the Pluronic micelles are disrupted and absorbed into the charged membrane, the hydrophilic PEO segments were depleted towards the membrane surface, retaining the drugs within. Overall, the CG-MD framework yields a detailed molecule-scale picture of the cooperative coulombic and amphiphilic effects, between charged moieties in contact with membrane surfaces.

1. Introduction

Medical theragnostic combines therapy and diagnosis into tailor-made personalized treatment. Liquid polymers, metal, mesoporous silica, or carbon-based nanoparticles[1,2] can be used as drug nanocarriers for this approach, yet undesired drug leaks[3] and multi-drug resistance remain important issues to be addressed.[4]

Micellar solutions of copolymers exhibit large potential,[5,6] promoting the solubilization of many, naturally hydrophobic, antitumoral drugs together with the possibility of ad-hoc chemical functionalizations. This feature has opened the door for targeting specific drugs[7] besides being able to trigger the drug release.[8] Many researchers focused on micellar solutions of triblock copolymers, known as Pluronic or Poloxamers,[9,10] as nanocarriers. These can accommodate antitumoral drugs either in their micelle cores (PPO) or on the hydrophilic (PEO) micelle coronas. Besides their biological compatibility, Pluronic micelles exhibit a relatively short storage time in the blood stream and possess a natural tendency to accumulate in tumorous regions.[2,11–13] The most appropriate Pluronic to be used as drug nanocarriers are F127, P123 or F68, which exhibit diverse hydrophilic/lipophilic balances (HLB) and can solubilise a wide range of antitumoral drugs such as doxorubicin (DOX) or gemcitabine (GEM). Further, mixing diverse HLB Pluronic moieties yields cross-micelles entailing distinct thermodynamic properties that can enhance drug loading/release capacities.[14] In contrast, Xu et al.[15] demonstrated that phenyl boric acid-modified Pluronic F127 mixed with P123-DOX loaded micelles, improved the antitumoral treatment in breast cancer MCF-7/ADR cells exhibiting improved stability and a high release rate.

The HLB of Pluronic can be controlled by the PEO/PPO ratio and their mutual arrangement in sequences of PEO-PPO-PEO (normal) or PPO-PEO-PPO (reverse). The equilibrium of Pluronic micelles relies on temperature and concentration conditions, the presence of salts or other copolymers, and ionic surfactants. Furthermore, the possibility of PEO functionalization can yield micelles for specific drugs.[13] These factors generate a unique platform for drug encapsulation and transport throughout fluids.[6,16–18]

Premature drug leaks may yield strong side effects which may produce more damage than the disease itsef. For instance, an uncontrolled DOX release was found in star-shaped copolymer micelles,[19] where the drug, in the PEO-water micelle surface was, excessively exposed to the environment. However, after chemical functionalisation, the same micelles were able to retain DOX closer to their micelle cores, protecting them until release.[19] Disclosing interactions between Pluronic nanocarriers and biological membranes is crucial for improving theragnostic treatment.

Another important issue in chemotherapy is multi-drug resistance (MDR) [4,20] which relies on the capacity of tumoral cells to overcome the action of antitumoral drugs. Despite a considerable effort, most studies on premature drug leaks and MDR issues are modelling studies[21] and trial/error experiments.[12] In silico techniques are able to tackle complex scenarios,[22] providing clues to interpret conflicting results[16–18] whilst providing molecular level details onto drug/host interactions.[23,24] Unfortunately, the intrinsic complexity of the problem has resulted in either the study of specific scenarios or the use of *ad-hoc* models with limited transferability.[25–29]

In this study, a coarse-grain molecular dynamics (CG-MD) computer simulation framework, based on the transferable MARTINI 2.2 force field (MF22),[22] was developed aiming at understanding the interplay between drugs and nanocarriers with biological membranes. The M2FF was selected due to its ability to tackle a great variety of biological systems, from DNA and big proteins to entire cells and virus envelopes.[21,22] We studied two nanocarriers, the cationic $G5^+$ PAMAM dendrimer and two nonionic P123 and F68 Pluronic, and two drugs, the amino deprotonated DOX^+ and neutral GEM antitumoral drugs. Two biological phospholipid membranes were chosen; the anionic 1-palmitoyl-2-oleoyl-glycero-3-phosphocholine POPC + 1-palmitoyl-2-oleoyl POPG (4-POPC:1-$POPG^-$) to model tumoral cell walls and dipalmitoyl phosphatidylcholine (DPPC), related to the infection of adenocarcinoma human alveolar lung tissue cells. We aimed to provide a comprehensive analysis of 4-POPC:1-$POPG^-$ and DPPC membranes with cationic $G5^+$ dendrimers and nonionic Pluronic micelles as nanocarriers preloaded with DOX^+ and GEM.

2. Methodology

2.1. Simulation details and molecular modelling

CG-MD simulations were performed with GROMACS 2023[30] using the leapfrog algorithm[31] to integrate the equations of motion with a 20 fs time step. The Lennard-Jones (LJ) potential and the Coulombic term with the potential-shift-verlet modifier and a cut-off radius of 1.2 nm were used. The long-range electrostatic interactions were computed with the Particle-Mesh-Ewald

(PME).[32] Bond stretching was constrained with the LINear Constraint Solver (LINCS).[33] The temperature was fixed to 303K using the velocity-rescaling thermostat[34] with a coupling time constant of τ_T = 1.0 ps. The pressure was fixed to 1 bar and controlled with the Parrinello-Rahman barostat[35] using a semi-isotropic pressure coupling with a time constant of τ_P = 24.0 ps.

G5 dendrimer[36], P123 and F68 Pluronic,[37] DOX,[38] GEM,[39] DPPC and 4-POPC:1-POPG and DPPC[40] membranes parameterization was taken from literature and can be consulted in **Figure S1**. The Packmol[41] code was used to build the simulation boxes. Periodic boundary conditions in all directions were used. Simulation snapshots were rendered with the Visual Molecular Dynamics (VMD) software package.[42]

The procedure to build each system was as follows; first, aqueous solutions with the different nanocarriers in contact with drugs (DOX^+ or GEM) were run. For instance, two simulation boxes with an aqueous solution of four $G5^+$ dendrimers each, including 20 DOX^+ or 20 GEM, respectively, were set. Then, the systems were equilibrated until all drugs were loaded in the $G5^+$ dendrimers. The membranes were built with the *insane* python code[43] and equilibrated with respect to the expected area per lipid (ApL). The MEMBplugin 1.1[44] tool available in the VMD software package[42] was used to obtain the ApLs for the DPPC, 55 $Å^2$ ($\pm$ 1) and 61.5 $Å^2$ ($\pm$ 1) for the 4-POPC:1-POPG membranes. These values are in reasonably good agreement with previous, experimental and computational, values, namely ~ 62 $Å^2$ ($\pm$ 6)[45–47] for DPPC and ~ 60 $Å^2$ ($\pm$ 3)[46–48] for 4-POPC:1-$POPG^-$.

The Packmol code was used to set the membrane (DPPC or 4-POPC:1-$POPG^-$) at the top of the simulation box closed to drug-loaded $G5^+$ dendrimers, which were previously equilibrated, and filled with water for the the selected concentrations (see **Table S1**). A similar procedure was followed to construct the three Pluronic P123, F68 and 1:1 P123/F68 micellar solutions at 5%wt. of concentration in water. Each system was equilibrated until their micellar size distributions matched previous studies.[49–51] Then, each micellar solution was brought into contact with 20 DOX^+ or 20 GEM until all drugs were loaded in the micelles or the system equilibrated. Afterwards, they were brought in contact with the membranes previously built and equilibrated as described for the $G5^+$ dendrimer. A summary of all simulation runs may be found in **Table S1**.

The simulation protocol, prior production runs, comprised an initial energy minimization, with the steepest descent algorithm, followed by successive 20 ns NVT and NpT equilibrations to set the proper temperature and density, respectively. The equilibrium was assessed on each step by ensuring that the temperature and density attained the equilibrium besides a visual inspection of the simulation snapshots prior the NpT production runs simulated along 8000ns.

Simulation trajectories were used to analyse solvent accessible surface areas (SASA), obtained with the *gmx sasa* GROMACS tool, to investigate the hydration/dehydration of different moieties along the simulation. Radial distribution functions were also obtained, with the *gmx rdf* GROMACS tool, to provide a quantitative perspective of contacts between membranes and nanocarriers whilst drug load/release capacities. The *gmx mindist* GROMACS tool was used to evaluate the number of drug-water, drug-membrane, and drug-carrier contacts to offer a qualitative comparison of the released drugs and whether these are in the membrane or in the water phase over time.

3. Results and Discussion

3.1. Dipalmitoyl phosphatidylcholine DPPC membrane

Figure 1 shows the final configuration for the nanocarriers solutions loaded with DOX^+ and GEM in contact with the DPPC membrane. **Figures 1a** and **1b** display the solution with four $G5^+$ dendrimers loaded with DOX^+ and GEM, respectively. Despite the $G5^+$ dendrimers reached the membrane in both solutions, only the $G5^+/DOX^+$ system released and transferred drugs, if few, into the membrane surface. Conversely, in the $G5^+$/GEM solution, GEM was partially released to the water phase instead as shown in **Figure 1b**. Since DPPC is uncharged, only dispersion interaction forces come into a play when $G5^+$ dendrimers reach the membrane. Since GEM is more hydrophilic than DOX^+, GEM transference into the membrane was found to be difficult, in line with experimental observations.[52] **Figure 2** shows the number of contacts between the drugs and nanocarriers (purple), the DPPC surface (red) and water molecules (blue) for the first 500 ns of simulation time. DOX^+ was found to decrease the contact with water and slightly augment the contact with $G5^+$ dendrimers. Contacts with the membrane surface remained stable and values well below those with $G5^+$ dendrimers and water molecules, meaning a poor DOX^+ release into the membrane, were found. For $G5^+$ loaded GEM, GEM contacts with $G5^+$, membrane or water remained stable (linear trend) during the first 300 ns, but a slight increase of contacts between GEM and water and GEM with the membrane surface whilst losing contacts with $G5^+$ (decay of the purple line). This suggests that some GEM were released to the water phase, reaching, some of them, the membrane surface (slight slope increase in the red line in the last 100 ns), **Figure 2b**, thus depicting a scenario similar to the simulation of **Figure 1b**. The number of contacts along 8000 ns of simulation indicates that both systems remained in equilibrium, **Figure S2**.

Figures 1c and **1d** illustrate the behaviour of P123 micelles in contact with DPPC when are loaded with DOX^+ and GEM, respectively. P123 micelles mostly retained all DOX^+ close to their PPO hydrophobic cores, **Figure 1c**, as also corroborated by the decrease of contacts between DOX^+ and P123 micelles and water as can be seen in **Figure 2c**. Meanwhile, DOX^+ contacts with the DPPC membrane surface increased, indicating an absorption of DOX^+ into the membrane surface. This could be because one of the P123 micelles was disrupted and P123 moieties were absorbed into the membrane. In this process, some DOX^+ were released into the membrane surface, yet most of P123/DOX^+ micelles remained in the aqueous solution. Conversely, **Figure 1d** shows that P123/GEM micelles were quickly dissolved and P123 moieties were absorbed by the membrane, with most of GEM attached to the P123 PEO segments, thus, being retained close to the membrane surface. This can be also seen in **Figure 2d** where GEM contacts with P123 rapidly decreased whereas augmented with water. However, hydrophilic interactions between GEM and PEO groups of P123 prevented GEM from being absorbed into the membrane surface as can be seen in **Figure 1d** and conveyed by the linear trend of GEM and membrane surface contacts variation (red line) along the simulation. **Figure S2** highlights this fact since the number of GEM contacts with water stedealy increased up to 1500 ns, where it reached equilibrium.

Figure 1e displays the hydrophilic F68 micelles loaded with DOX^+ which were mainly located between F68 micelles and the surface of the membrane. Interestingly, one of the F68 micelles was disrupted and F68 moieties were absorbed as observed in the P123 solution (**Figure 1c**). **Figure 2e** shows that during the first 100 ns, the number of DOX^+ contacts with F68 and water decreased whereas the number of DOX^+ contacts with the DPPC membrane surface (red line) increased. Above 500 ns, the number of contacts reached equilibrium, as shown in **Figure S2**. A different picture emerged when F68 micelles were loaded with GEM which remained attached to the PPO of the micelle cores. One of the F68 micelles was disrupted but the released GEM was retained by the remained F68 micelles but not linked to the membrane surface as happened in F68/DOX^+ (**Figure 1f**). **Figure 2f** confirms this behaviour with a slight decrease of contacts between GEM and F68 and an increase with water during the first 50 ns. GEM contacts with DPPC membrane were very low and constant as shown in the results of the simulation snapshot of **Figure 1f**. The contacts remained in equilibrium along 8000 ns of simulation time, **Figure S2**.

Figures 1g and **1h** show P123/F68 mixed micelles with loaded DOX^+ and GEM, respectively. **Figure 1g** shows that most of DOX^+ remained attached to the P123/F68 mixed micelles though one of them was disrupted and absorbed by the membrane retaining all DOX^+ within and facilitating their contact with the membrane. **Figure 2g** displays a slight increase of DOX^+ contacts with the DPPC membrane along the first 300 ns of simulation time while barely decreasing with P123/F68 micelles and slightly more noticeable was the decrease with water. **Figure 1h** displays the solution with GEM, indicating an intermediate behaviour between the P123 and F68 micellar solutions where one of the P123/F68 micelles was dissolved and absorbed into the membrane (as in **Figures 1d** and **1f**). Nevertheless, the solution with P123/F68 mixed micelles retained some GEM within and close to the membrane surface, conversely to what found with pure F68 micelles (**Figure 1f**). **Figure 2h** supports this, showing a noticeable number of contacts between GEM and the DPPC membrane which is due to the initial close contacts between P123/F68 loaded micelles and the membrane, since no GEM release was observed. Those contacts rapidly decreased during the first 300 ns, remaining stable afterwards, with similar values for the contacts between GEM and the membrane, the P123/F68 micelles and water molecules. The number of contacts between GEM and P123/F68 barely changed (purple line), denoting that GEM was not released and remained stable, as also shown in **Figure S2** where the number of all contacts remained in equilibrium above 500 ns.

Videos of all the solutions from different perspectives of the final configurations can be found in the SI section (**MS1**). These show DPPC membrane headgroups (to highlight the membrane surface), drugs, counterions and nanocarriers for a clearer view aiming to highlight the interactions between nanocarriers, drugs and membranes.

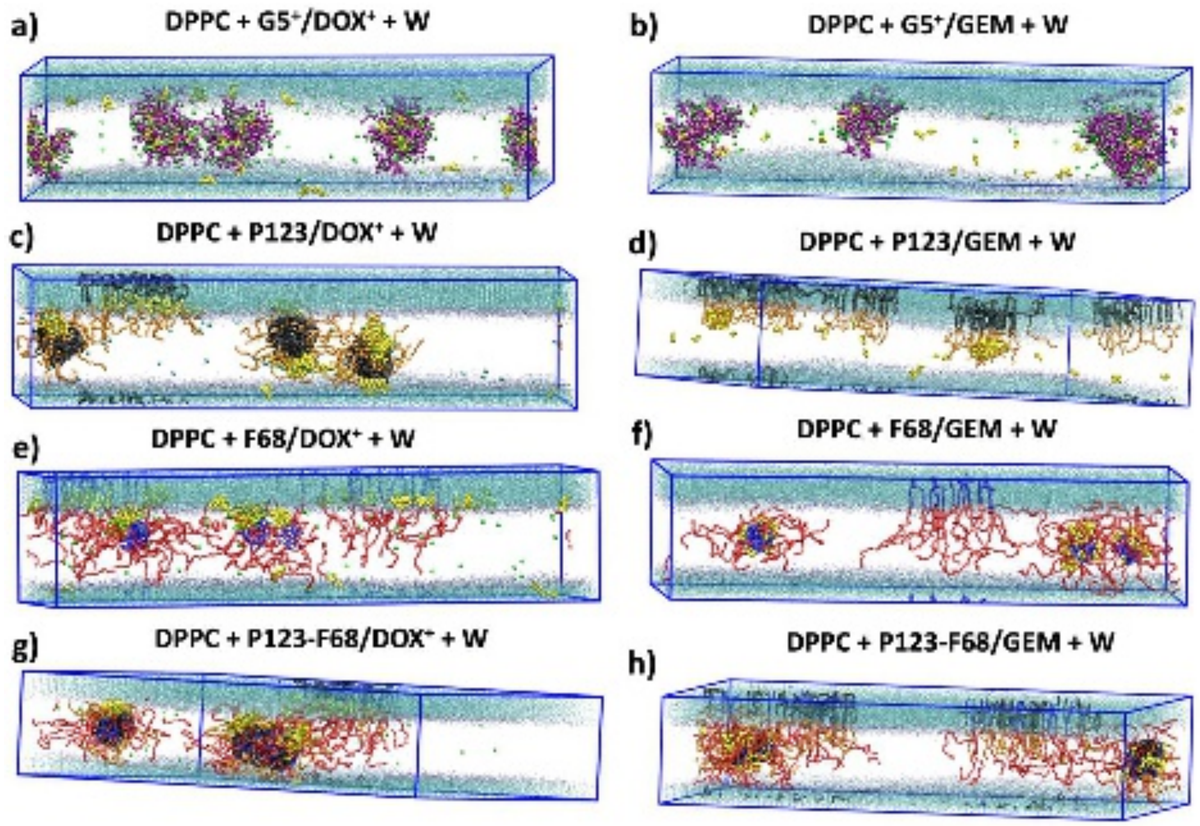

Figure 1. Simulation snapshots after 8000 ns of simulation time for the selected nanocarriers preloaded with DOX^+ or GEM in contact with the DPPC membrane. a) $G5^+/DOX^+$, b) $G5^+$/GEM, c) P123/DOX^+, d) P123/GEM, e) F68/DOX^+, f) F68/GEM, g) P123-F68/DOX^+ and h) P123-F68/GEM. The colour code is as follows; $G5^+$ dendrimers in purple, DOX^+ (left) and GEM (right) in yellow, PPO Pluronic groups in black and blue for P123 and F68 micelles, respectively whereas PEO groups are coloured in orange and red for P123 and F68 micelles, respectively. DPPC molecules are depicted as small blue and purple dots. Chlorides were coloured in green whereas water was removed for clarity.

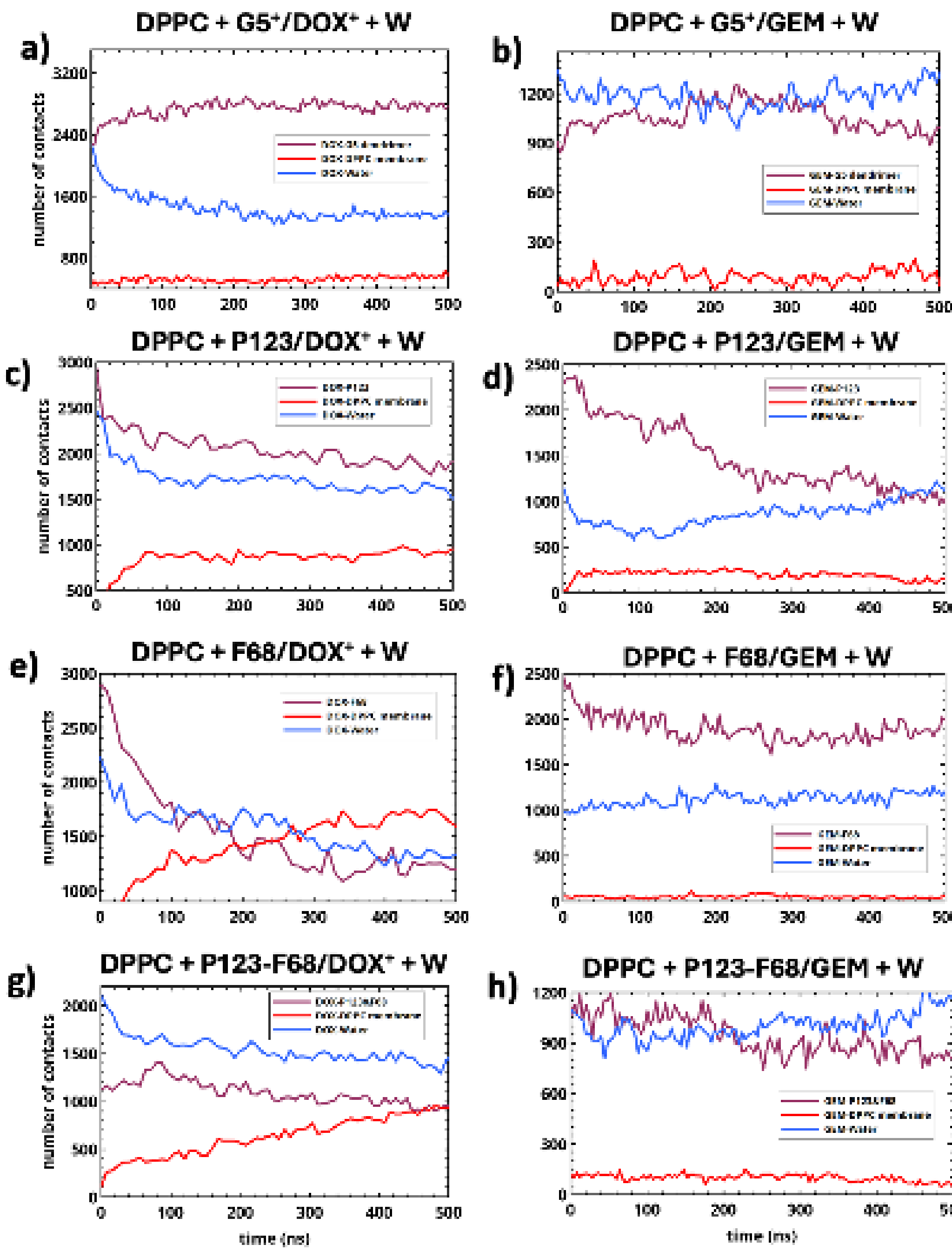

Figure 2. Number of contacts for the first 500 ns between drugs and their nanocarriers (purple), drugs and water (blue) besides DPPC membrane surface and drugs (red) for the DPPC membrane with a) G5$^+$/DOX$^+$, b) G5$^+$/GEM, c) P123/DOX$^+$, d) P123/GEM, e) F68/DOX$^+$, f) F68/GEM, g) P123-F68/DOX$^+$ and h) P123-F68/GEM.

3.2. 1-palmitoyl-2-oleoyl-glycero-3-phosphocholine 4-POPC + 1-palmitoyl-2-oleoyl POPG membrane

Figures 3a-h display the final simulation snapshots for DOX^+ and GEM-loaded nanocarriers in contact with anionic 4-POPC:1-$POPG^-$ membrane. **Figure 3a** highlights a noticeable folded assembly of the membrane likely due to the increased number of charged species. In contrast with the neutral DPPC membrane –despite possessing charged headgroups, they are counter-balanced exhibiting zero net charge– the 4-POPC:1-$POPG^-$ membrane surface is constituted by two distinctive phospholipid headgroups: a bulkier phosphatidylcholine (PC) and an anionic phosphatidylglycerol (PG^-) group. In aqueous solution, 4-POPC:1-$POPG^-$ membranes exhibit flattened structures.[53] However the membrane can bend and fold when charged species are present as observed in experimental and theoretical studies. Therefore, the increased interactions of ionic species with the 4-POPC:1-$POPG^-$ membrane surface can yield more energetically favourable curved structures.

Confirming this, the cationic character of $G5^+$ dendrimers promoted highly corrugated structures as shown in **Figures 3a** and **3b**. **Figure 3a** indicates that some DOX^+ were released and attached to the membrane surface whereas others were still enclosed to $G5^+$ dendrimers. A more quantitative picture is provided in **Figure 4** displaying the number of contacts, as previously done for the DPPC membrane (**Figure 3**). **Figure 4a** shows how DOX^+ lost contacts with water meanwhile they were slightly increased with the 4-POPC:1-$POPG^-$ membrane surface (red line), denoting a modest drug release into the membrane surface corroborated by the linear pattern of the number of contacts between DOX^+ and $G5^+$. **Figure 3b** shows a similar scenario but GEM was dissolved as shown with the topmost GEM contacts shown in **Figure 4b** (blue line). **Figure 4b** also confirms that the number of contacts barely changed in the first 500 ns and above, and remained mostly stable along 8000 ns as can be seen in **Figure S3**.

Figures 3c and **3d** illustrate the behaviour of P123 micelles loaded with DOX^+ and GEM, respectively. **Figure 3c** shows that practically all P123/DOX^+ micelles were disrupted and released DOX^+ were arranged in some regions of the membrane surface, promoting bent structures – though less prominent than with $G5^+$ dendrimers. Only one P123 micelle survived and was linked to the membrane surface, retaining some DOX^+ within. **Figure 4c** exhibits a clear decrease of DOX^+

contacts with P123 and water whereas increased with the membrane surface (red line). Above 500 ns, the number of contacts remained stable, pointing out that the equilibrium was attained as also shown in **Figure S3**. A different scenario was observed in the P123/GEM solution (**Figure 3d**) where the 4-POPC:1-POPG$^-$ membrane preserved its original flattened structure, likely due to the presence of less ionic species, but all micelles were dissolved and P123 moieties absorbed into the membrane. Released GEM remained in the water phase and some close to the membrane surface as noticed by the slight increase in the number of GEM-water and GEM-membrane contacts (**Figure 4d**) whereas GEM-P123 contacts drastically decreased. **Figure S3** indicates that the number of contacts reached the equilibrium above 500 ns. **Figure 3d** displays how GEM formed small clusters instead of remaining linked to PEO P123 segments as occurred with the DPPC membrane (**Figure 1d**). This could be due to the presence of Na^+ cations that were arranged around the anionic PG$^-$ headgroups of the membrane surface. In fact, Na^+ species could screen the interactions between PEO and GEM as also observed with the DPPC membrane.

Figures 3e and **3f** show a total dissolution of F68 micelles loaded with both, DOX$^+$ and GEM, respectively. After micelle disruption, absorbed F68 moieties were arranged with all PEO groups facing the water phase and retaining the released DOX$^+$ close to the membrane surface. **Figure 4e** shows an important decrease of DOX$^+$ contacts with F68 micelles and water meanwhile are increased with the membrane surface (red line) in the first 100 ns. In contrast to the other systems, this solution required 1500 ns to reach the equilibrium as noticed by the stable number of contacts shown in **Figure S3**. Conversely to G5$^+$ dendrimers and P123 micelles solutions, the 4-POPC:1-POPG$^-$ membrane was barely distorted in the presence of F68, pointing towards more stable structures. F68 micelles loaded with GEM (**Figure 3f**) displayed the same behaviour as P123 micelles, yielding a stable and flat 4-POPC:1-POPG$^-$ membrane structure with all of the initial F68 micelles disrupted and moieties absorbed into the membrane. Released GEM can be mainly found in the water phase as can be seen in **Figure 4f** with the increased number of GEM-water contacts (blue line) whereas a decrease in GEM-F68 contacts being GEM-membrane ones maintained, at least during the first 200 ns. Notably, those contacts were decreased afterwards, likely because of the formation of small GEM clusters as shown in **Figure 3f**. This solution also required at least 1500 ns to reach the equilibrium (**Figure S3**) as also observed with the F68/DOX^+ micelles.

Conversely, P123/F68 mixed micelles loaded with DOX^+ and GEM promoted strongly bent membrane structures as illustrated in **Figures 3g** and **3h**. Nevertheless, mixed micelles were less prone to be disrupted, conversely to what was observed in P123 and F68 solutions. In the case of P123/F68 loaded with DOX^+, only two of the original micelles were dissolved whereas the other two remained intact and they were located close to the membrane surface with DOX^+ closely linked between the membrane surface and the linked micelles as can be noticed in **Figure 3g**. This complex scenario can be rationalized by the number of contacts displayed in **Figures 4g** and **4h** denoting similar trends between drugs-P123/F68 micelles and membrane-water. In fact, **Figure 4g** illustrates a quick increase of DOX^+ contacts with the membrane (red line) while slightly decreasing with P123/F68 micelles and water molecules. This trend could be caused by the close connection between the P123/F68 micelles and the highly corrugated 4-POPC:1-$POPG^-$ membrane as illustrated in **Figure 3g**. This solution seems to be stable above 200 ns, as also shown in **Figure S3**.

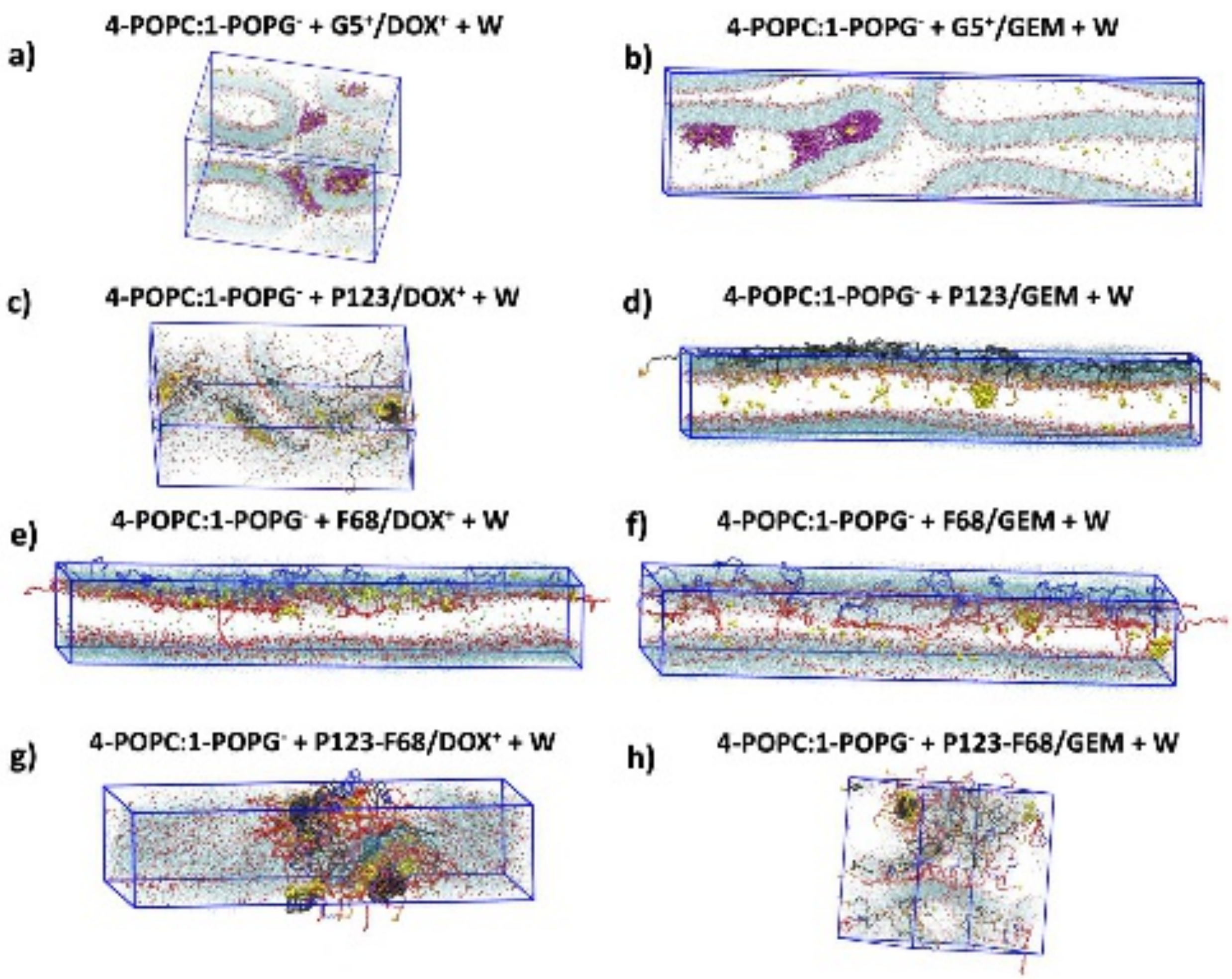

Figure 3. Simulation snapshots after 8000 ns of simulation time for the selected nanocarriers preloaded with DOX^+ or GEM in contact with the 4-POPC:1-POPG⁻ membrane. a) $G5^+/DOX^+$, b) $G5^+$/GEM, c) P123/DOX^+, d) P123/GEM, e) F68/DOX^+, f) F68/GEM, g) P123-F68/DOX^+ and h) P123-F68/GEM. The colour code is the same as in **Figure 1** with 4-POPC:1POPG⁻ molecules depicted as small blue and purple dots. Chlorides and sodium were coloured in small green and red dots, respectively whilst water was removed for clarity.

Figure 3h shows a similar scenario but only one P123/F68 micelle survived, and it was arranged close to the membrane surface (still loaded with GEM) whereas the other three micelles were dissolved with GEM released and yielding some small clusters in the water phase as also observed in the P123 and F68 micellar solutions. The profiles in **Figure 4h** suggests an analogous situation with DOX^+, with a quick increase (first 100 ns) of GEM contacts because of the highly corrugated 4-POPC:1-POPG⁻ structure. **Figure S3** shows that the system was stabilised above 800 ns. When mixed P123/F68 micelles are compared with P123 and F68 ones, simulation results (**Figure 4**) indicate a drop in drug release into the membrane surface when compared with the hydrophobic P123 and hydrophilic F68 micellar solutions. A brief comparison of the trends in **Figures 4c-4h** implies a sharper increase/decrease of the number of contacts in P123 or F68 solutions when compared with P123/F68 ones. A general perspective of the final configurations can be consulted as a movie in the SI section (**MS2**). The movies included 4-POPC:1-POPG$^-$ membrane headgroups (membrane surface), drugs, counterions and nanocarriers for a clearer view.

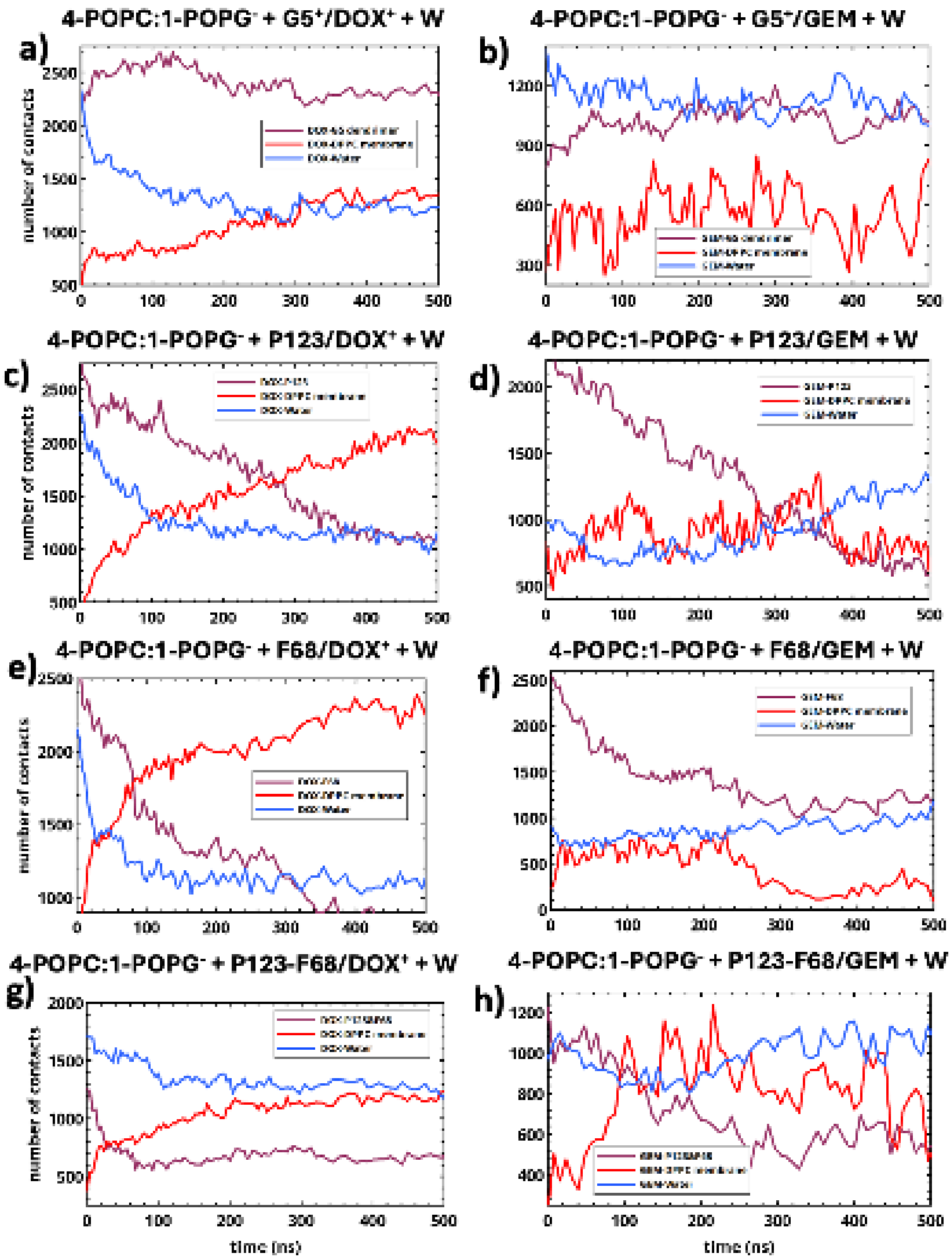

Figure 4. Number of contacts for the first 500 ns between drugs and their nanocarriers (purple), drugs and water (blue) besides 4-POPC:1-POPG$^-$ membrane surface and drugs (red) for the 4-POPC:1-POPG$^-$ membrane with a) G5$^+$/DOX$^+$, b) G5$^+$/GEM, c) P123/DOX$^+$, d) P123/GEM, e) F68/DOX$^+$, f) F68/GEM, g) P123-F68/DOX$^+$ and h) P123-F68/GEM.

3.3. A close perspective of drug arrangement

Figure 5 displays the radial distribution functions (RDF) of drugs and phospholipid head groups of the membrane surface. **Figure 5a** shows the RDF between DOX$^+$ and the phosphatidylcholine (PC) head groups of the DPPC membrane overall nanocarrier solutions. A comparison of the RDFs reveals where the released drugs were arranged along the simulation. The relatively hydrophilic F68 micelles allowed more DOX$^+$ (blue line) to stay in contact with the membrane surface, followed by P123, P123/F68 and G5$^+$ dendrimer solutions. This is confirmed by the visual analysis of the simulation snapshots (**Figure 1**). DOX$^+$ formed small clusters over the DPPC membrane surface in the solution with F68 micelles. Conversely, the solutions with G5$^+$ dendrimers or P123/F68 micelles, DOX$^+$ was mainly retained, although a few of them were released into the water phase. This trend was inverted when GEM is considered (**Figure 5b**). P123 micelles noticeably released more GEM in the membrane surface than G5$^+$, P123/F68 and F68, respectively (as also found in the final configurations **Figure 1d**). The P123 micelles were all disrupted, and moieties absorbed into the membrane while retaining all GEM linked to the P123 PEO segments which protrude from the membrane surface. **Figure 5b** also indicates that P123/F68 micelles barely released GEM, which could be caused by the dissolution of one of the micelles (**Figure 1h**), whereas hydrophilic F68 micelles practically retained all GEM within as shown in **Figure 1f**.

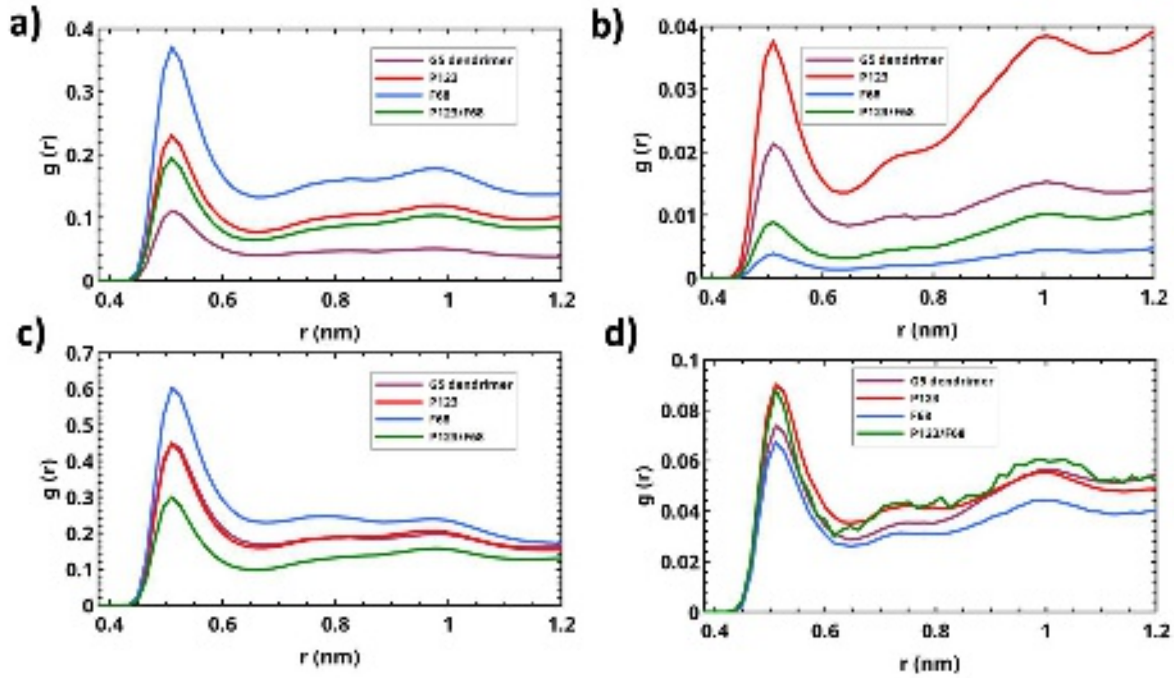

Figure 5. Radial distribution functions (RDF) between DOX$^+$ (left) and GEM (right) with phosphatidylcholine (PC) head groups of the DPPC (a and b) and PG$^-$ head groups of the 4-POPC:1-POPG$^-$ membrane surface (c and d).

Figures 5c and **5d** compare the RDF between DOX$^+$ and the PC and the PG$^-$ head groups of the 4-POPC:1-POPG$^-$ membrane. **Figure 5c** exhibits a similar trend as the DPPC membrane but slightly higher intensities overall nanocarriers, indicating increased contacts of DOX$^+$ with the membrane surface. A quick F68 micelle disruption yielded F68 moieties being absorbed into the membrane retaining DOX$^+$ within, as observed in the simulation snapshot (**Figure 3e**). P123 micelles also released practically all DOX$^+$ but not all micelles were disrupted, with one of them retaining some DOX$^+$ within the micelle core. P123/F68 micelles and G5$^+$ dendrimers showed a similar DOX$^+$ release though the behaviour of both nanocarriers was different. The G5$^+$ dendrimers were not dissolved and absorbed into the membrane as occurred with the P123, however, the similarities observed in the RDFs arise from structural deformations of the 4-POPC:1-POPG$^-$ membrane, noticeable corrugated in the solution with G5$^+$ dendrimers due to the increased number of charged species in the solution.

The anionic character of the 4-POPC:1-POPG$^-$ membrane surface yielded a different DOX$^+$ release when compared with the solution in contact with the neutral DPPC membrane. Attractive coulombic interactions between cationic G5$^+$ dendrimers and anionic PG$^-$ groups of the 4-POPC:1-

POPG$^-$ membrane promoted their contact, yielding a greater structural change in the membrane, **Figures 1a** and **3a**. The P123/F68 solution barely released DOX$^+$ where micelles remained intact, and DOX$^+$ was kept inside their cores. The presence of ionic species could be behind the structural changes in the membrane as occurred in the solutions with G5$^+$ dendrimers and P123 micelles but less noticeable as shown in **Figures 3a, 3c** and **3g**.

A different picture was observed with GEM, for which the relatively hydrophobic P123 and P123/F68 micelles increased GEM release compared with the hydrophilic F68 and G5$^+$ nanocarriers, exhibiting both the highest RDF intensity peaks (**Figure 5d**). Inversely, GEM release from F68 was less prominent despite all micelles being dissolved and absorbed in the membrane. Released GEM formed some small clusters, but they seem weakly linked to the membrane surface compared with other solutions, conveyed by the lowest RDF intensity peak (**Figure 5d**). The counter ions played an important role since their arrangement and concentration impact the membrane structure and interactions with drugs and nanocarriers. **Figure S4** displays the RDF of Cl$^-$ with respect to PC headgroups of the DPPC membrane for all nanocarriers loaded with DOX$^+$. The G5$^+$ dendrimer loaded with GEM was also considered due to the cationic character of G5$^+$. The RDFs in **Figure S4** show a noticeable presence of Cl$^-$ close to the DPPC surface in the solutions with F68 and P123 micelles but diminished in the P123/F68 and G5$^+$. This resembles the RDF intensity peak trend shown in **Figure 5a** where DOX$^+$, located in the DPPC surface, follows F68 > P123 > P123/F68 > G5$^+$. **Figure S4** highlights the role of coulombic interactions between Cl$^-$ and DOX$^+$, directing the distribution of the counterions. In fact, Cl$^-$ was placed closer to the DPPC membrane surface in the solution with G5$^+$ dendrimers loaded with GEM. Since GEM is neutral, Cl$^-$ can freely move in the solution and be arranged closer to the membrane as indicated by the higher RDF (**Figure 5b**). The 4-POPC:1-POPG$^-$ membranes usually form flattened or slightly bent structures in aqueous solution. **Figure S5a** shows the DPPC membrane in solution under the same conditions as the systems with the nanocarriers. This membrane retained the original flat structure after 8000 ns. However, our 4-POPC:1-POPG$^-$ membrane exhibited some curvature as can be seen in **Figure S5b**.

Charged membranes, as 4-POPC:1-POPG$^-$, possess an increased rigidity when compared with neutral ones such as the DPPC. However, the presence of ionic species, Na$^+$ and Cl$^-$, in solution that counterbalances the anionic PG$^-$ headgroups and cationic species (G5$^+$), respectively, can yield destabilisation and/or bent structures. Faizi et al.[54] compared experiments and theory to characterise the rigidity and bending properties of 4-POPC: 1-POPG$^-$ membranes, claiming that the rigidity of the membrane surface is reduced by the presence of monovalent ions in solution due to the electrostatic screening when Na$^+$ sits close to the PG$^-$ groups of the membrane surface. Further, they suggested that theoretical models may overestimate the bending rigidity at intermediate fractions of the charged lipid (our 4-POPC: 1-POPG$^-$ membrane) in the absence of NaCl. Besides the coulombic nature of the membrane surface, Dickey and Faller[53] argued that the size of the phosphatidyl-based headgroups can impact the structure of the membrane surface but the stability of the membrane relies more on Na$^+$ location at the membrane surface. To shed light on the role of Na$^+$ arrangement at the surface of the 4-POPC: 1-POPG$^-$ membrane, the RDF between Cl$^-$ and Na$^+$ with PC and PG$^-$ groups of the 4-POPC:1-POPG$^-$ membrane surface were displayed in **Figure 6**.

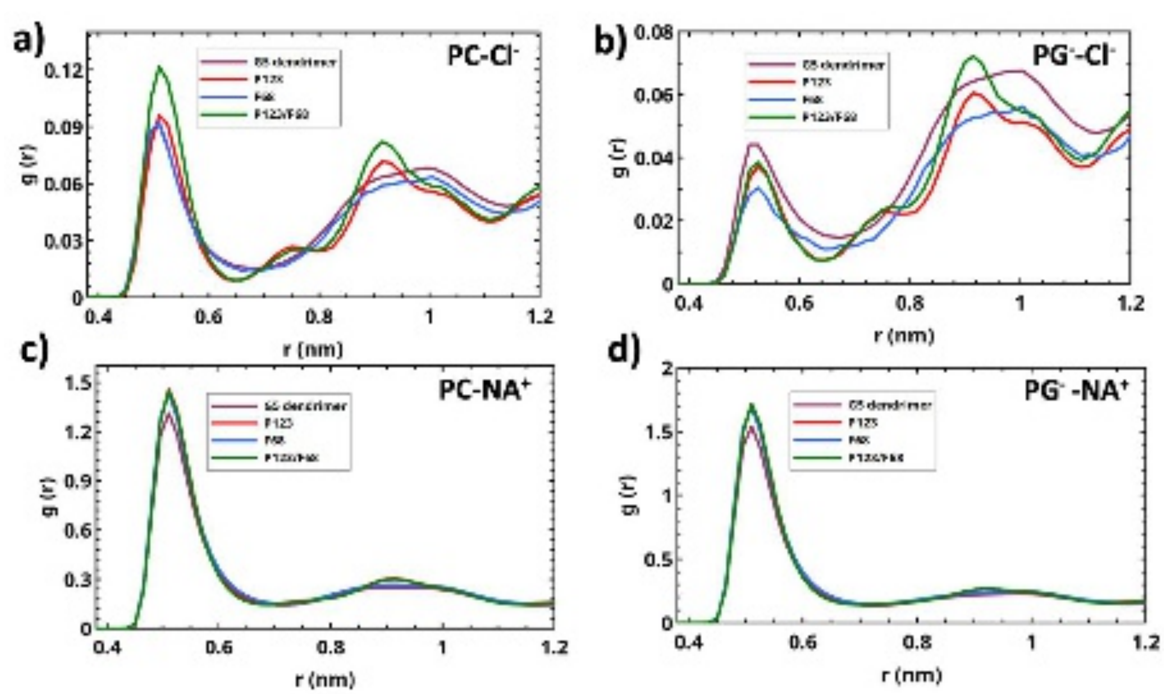

Figure 6. Radial distribution functions (RDF) averaged over 8000 ns of simulation for Cl$^-$ and Na$^+$ ions with respect to the phosphatidylcholine PC and phosphatidylglycerol PG$^-$ head groups of the 4-POPC:1-POPG$^-$ membrane surface overall nanocarriers loaded with DOX$^+$. The RDF profiles are distributed as follows: a) PC-Cl$^-$, b) PG$^-$-Cl$^-$, c) PC-Na$^+$ and d) PG$^-$-Na$^+$.

Figures 6a and **6b** present the RDF between Cl^- and the PC and PG^- groups of the 4-POPC:1-$POPG^-$ membrane overall nanocarriers loaded with DOX^+. The P123/F68 solution shows slightly more Cl^- anions around neutral PC groups as can be seen in **Figure 6a**. The Cl^- ions were preferably arranged around PC groups since the RDF of PG^- groups are almost depleted, denoting that most Cl^- ions are in the water phase as displayed in **Figure 6b**. **Figures 6c** and **6d** show the distribution of Na^+ between PC and PG^- groups, respectively, exhibiting similar trends. The intensity of the first maximum peak highlights the preference of Na^+ to arrange in the membrane surface rather than in water, conversely to Cl^- ions (**Figures 6a** and **6b**), with no preference between PC or PG^- groups. **Figure 6** also shows that Cl^- distribution around PC and PG^- groups in the solution with $G5^+$ dendrimers was like the Pluronic solutions. A low Na^+ concentration on the membrane surface was found around both PC and PG^- groups likely due to an increased number of Cl^-. Overall, Cl^- tended to stay close to PC groups whereas Na^+ were distributed equally in both, PC and PG^- groups. This asymmetry in the charge density distribution in the membrane surface could promote the 4-POPC:1-$POPG^-$ membrane surface curvatures as shown in **Figures 3a, 3c, 3e,** and **3g**. More details can be consulted in **Figure S6** with the RDF between Na^+ and the PC whilst PG^- groups of the 4-POPC:1-$POPG^-$ membrane overall nanocarrier solutions when loaded with GEM. Also, the hydration of selected moieties overall solution is discussed in **Figure S7**.

4. Overall outcomes

For overall nanocarriers in contact with neutral DPPC membranes, the cationic $G5^+$ dendrimers revealed a complicated scenario where DOX^+ mainly remained in the dendrimer and only some were released into the membrane surface. DOX^+ was absorbed into the surface of both membranes whereas GEM preferred to stay in the water phase forming small clusters in both systems as shown in **Figure S8**. For $G5^+$ dendrimers loaded with GEM, most of them were released into the water phase as observed without the nanocarrier. Conversely, Pluronic micelles seem a better solution if their hydrophilic-lipophilic balance is properly chosen. With DPPC membrane, F68 micelles exhibited enhanced features for transporting ionic drugs (DOX^+) but they were unable to release GEM. Even when some F68 micelles were dissolved, the GEM molecules were quickly captured by surrounding micelles, preventing them to remain in the aqueous medium as happens without nanocarriers as shown in **Figure S8b**. This is a good feature to avoid early drug leaks until a drug-release mechanism is triggered when reaching the target. P123 was more convenient for releasing GEM since all P123 micelles were dissolved and GEM molecules were kept close to the membrane surface due to GEM-PEO interactions. Despite all P123 micelles were disrupted and GEM were released, the absorbed P123 moieties were arranged inside the membrane but PEO segments facing the water face, gathering the previous released GEM and maintaining them close to the membrane surface rather than in water as happened when micelles are not present (**Figure S8b**).

In contact with the anionic 4-POPC:1-POPG$^-$ membrane surface, G5$^+$ dendrimers loaded with cationic DOX$^+$ and neutral GEM yielded important structural changes in the membrane. Also, P123 micelles loaded with DOX$^+$ generated a significant membrane bent, but retained its original flattened structure when loaded with GEM. In both solutions, P123 micelles were dissolved and Pluronic moieties were absorbed into the membrane. However, DOX$^+$ molecules were also incorporated in the membrane surface whereas the more hydrophilic GEM remained in the water phase, yielding small clusters as also shown when nanocarriers are not present (**Figure S8d**).

Figure S9 shows how the nanocarriers interact with the DPPC and 4-POPC:1-POPG$^-$ membranes when are not loaded with drugs. G5$^+$ was linked the membrane surface, being well surrounded by the Cl$^-$ counterions. The 4-POPC:1-POPG$^-$ membrane exhibits a slight curvature due to the increased number of ions in the solution when compared with the neutral DPPC. However, both membranes maintained the original shape, conversely to the twisted structures found when both drugs are present. Like solutions loaded with drugs, most of the Pluronic micelles were disrupted with Pluronic unimers absorbed into the membranes. This was more noticeable with Pluronic in contact with the anionic 4-POPC:1-POPG$^-$ membrane as can be seen in **Figures S9d**, **S9f**, and **S9h**. Compared with their drug-loaded counterparts, three of the original P123 micelles were dissolved and absorbed into the DPPC membrane for neat and DOX$^+$ loaded solutions. However, without DOX$^+$, the membrane remained intact whereas in the solution with DOX$^+$, the DPPC membrane was bent as can be seen in **Figure 3c**. If one compares **Figures S9b** and **3d**, in contact with the 4-POPC:1-POPG$^-$ membrane, the same scenario was found with and without GEM, with all micelles dissolved and moieties absorbed in the membrane. For solutions with F68, in contact with the DPPC membrane it was observed less micelle disruption when DOX^+ is loaded (**Figures S9e** and **3e**) but the same scenario was depicted when F68 micelles are in contact with the 4-POPC:1-$POPG^-$ membrane as can be noticed if one compares **Figures S9f** and **3f**, respectively. P123-F68 solutions also showed some differences when they are loaded with drugs. Whereas P123-F68 micelle disruption followed a similar pattern, no matter they are loaded with drugs or not, the solutions with drugs yield twisted membranes (**Figures 3g** and **3h**) in contrast with the flattened structures found in **Figures S9g** and **S9h**. Thereby, the presence of drugs could also contributes to the destabilisation of the membrane as happens with the counterions. Overall, the solutions with unloaded nanocarriers displayed more stable membranes but when they are used to deliver drugs, Pluronic seems less prone to modify the original structure of the membrane, especially in charged membranes such as 4-POPC:1-$POPG^-$.

When considering a proper drug nanocarrier to interact with biological membranes, the concentration of ionic species has an important role, not only in the structure of the membranes but also in the stability of the nanocarriers. The presence of Na^+ and Cl^- counterions modify the hydration properties of amphiphiles, included Pluronic, due to salt-in/out effects. Concretely, charged species impact the hydration of micelles coronas, even promoting phase transitions and altering their micellar size distributions. Further, the Pluronic nature has an important impact since Pluronic unimers exhibited a different behaviour when they are absorbed into DPPC or 4-POPC:1-$POPG^-$ membranes. Considering the solutions shown in **Figures 1c-h** and **2c-h**, the absorbed Pluronic unimers exhibited a different behaviour with PEO segments facing the water phase when they were absorbed in DPPC membrane whereas PEO segments were depleted towards the membrane surface in 4-POPC:1-$POPG^-$. A good example is P123 Pluronic loaded with GEM in contact with DPPC or 4-POPC:1-$POPG^-$ membranes displayed in **Figures 1d** and **2d**, respectively. The increased ionic concentration required in the 4-POPC:1-$POPG^-$ membrane yielded different hydration of P123 PEO segments. The Na^+ and Cl^- counterions were mainly arranged in the 4-POPC:1-$POPG^-$ membrane surface, yielding a dehydration of the absorbed P123 unimers which have hydrophobic PPO groups arranged well inside the lipidic core of the membrane whereas PEO were located at the membrane surface. Recently, a study by Kim et al.[55]

found that standard values for cutoffs, neighbour list updates, and time intervals in barostat updates might result in the neglect of pair interactions and unnaturally bent membrane structures. This is highly relevant for our study and was analysed in detail. First and relevantly, our reference models, **Figure S8** and **S9**, exhibit flat structures, where this should not be an issue. Furthermore, when two different systems with bent structures, 4-POPC:1-POPG$^-$ membrane + G5/GEM + W (**Figure 3b**) and 4-POPC:1-POPG$^-$ membrane + P123/DOX + W (**Figure 3c**), were computed with the parameters suggested by Kim et al. very similar structures were obtained (**Figure S10**). This indicates that this is not an issue in our study.

5. Conclusions

We show how MARTINI-based CG-MD simulations can tackle biological phospholipid membranes in contact with drug-loaded nanocarriers. The times and sizes made possible for this methodology, allowed us to treat several drug-loaded nanocarriers in contact with relatively large membrane surfaces in the μs regime and to observe relevant structural changes such as surface corrugation and micelle disruptions. Simulations revealed that neutral DPPC membranes are more stable overall nanocarriers, and the concentration of ionic species had a relatively low impact. Conversely, ionic moieties impact the anionic 4-POPC:1-POPG$^-$ membrane, displaying a variety of structural morphologies, including large membrane bendings in presence of ionic G5$^+$ dendrimers or mixed P123/F68 micelles. The charge landscape unbalance between the phosphatidylglycerol (PG$^-$) and phosphatidylcholine (PC) headgroups of the 4-POPC:1-POPG$^-$ membrane surface makes bent structures energetically favourable matching previous atomistic simulations[53] and experimental studies.[56] Therefore, both the absorbed Pluronic unimers and the concentration of counterions over the surface, disrupt the 4-POPC:1-POPG$^-$ membrane surface. However, when a more hydrophilic Pluronic is considered, F68, lower structural changes were observed. Furthermore, in this system loaded with DOX$^+$ and GEM, micelles were disrupted and unimers absorbed into the membrane. This is probably due to the relatively large hydrophilic PEO branches, which face and interact with water, and aid in the stabilisation of the membranes, which matched with experimental results showing that F68 micelles are less aggressive with biological membranes while retaining its drug loading/deliver capacities when compared with more hydrophobic Pluronic.[57]

Our simulations address the role of each moiety in the stabilisation during the transport and further release of drugs into biological membranes. The inherent general and transferable perspective of MARTINI opens the possibility for *in-silico* exploring novel taylor-made drug nanocarriers yet to be synthesised.

SUPPLEMENTARY MATERIAL

This section contains the movies MS1 and MS2 besides a summary of the simulation runs developed in this study including the CG-MD mapping for all compounds. A brief discussion addressing the number of contacts between molecules, solvent accessible surface areas and radial distribution functions along the entire simulation can be consulted. As a reference, **Figures S5, S8,** and **S9** display neat membranes, membranes + drugs and membranes + nanocarriers (unloaded), respectively. **Figure S10** shows a brief test of Kim et al.[55] suggested setup for the treatment of cutoffs, neighbour list updates, and barostat updates that could yield the missing of pair interactions yielding artifacts in the shape of the membrane.

Acknowledgments

This work was developed in CICECO-Aveiro Institute of Materials within the scope of the projects UIDB/50011/2020, UIDP/50011/2020 & LA/P/0006/2020 financed by national funds through the FCT/MEC (PIDDAC. G.P-S acknowledges the national funds (OE), Ref. DL 57/2016/CP1482/CT004 and DOI: 10.54499/DL57/2016/CP1482/CT0043 through FCT – Fundação para a Ciência e a Tecnologia I.P. in the scope of the framework contract foreseen in the numbers 4, 5 and 6 of the article 23 of the Decree-Law 57/2016 of August 29th changed by Law 57/2017 of July 19th. Simulations resources were financed by the FCT program "Concurso de Projetos de Computação Avançada - 4ª Edição" under a financed project with reference 2023.10643.CPCA.A2. Simulations were performed at the OBLIVION computer cluster facility managed by the HPC Centre of the University of Évora which was acquired under the “Enabling

Green E-science for the SKA Research Infrastructure (ENGAGE SKA)" reference POCI-01-0145-FEDER-022217 and funded by COMPETE 2020 and Foundation for Science and Technology (FCT), Portugal.

References

[1] S.M. Hosseini, J. Mohammadnejad, S. Salamat, Z. Beiram Zadeh, M. Tanhaei, and S. Ramakrishna, "Theranostic polymeric nanoparticles as a new approach in cancer therapy and diagnosis: a review," Mater Today Chem **29**, 101400 (2023).

[2] Y. Gregoriou, G. Gregoriou, V. Yilmaz, K. Kapnisis, M. Prokopi, A. Anayiotos, K. Strati, N. Dietis, A.I. Constantinou, and C. Andreou, "Resveratrol loaded polymeric micelles for theranostic targeting of breast cancer cells," Nanotheranostics **5**(1), 113–124 (2021).

[3] M. Gisbert-Garzaran, D. Lozano, M. Vallet-Regí, and M. Manzano, "Self-immolative polymers as novel pH-responsive gate keepers for drug delivery," RSC Adv **7**(1), 132–136 (2017).

[4] A. Catalano, D. Iacopetta, J. Ceramella, D. Scumaci, F. Giuzio, C. Saturnino, S. Aquaro, C. Rosano, and M.S. Sinicropi, "Multidrug Resistance (MDR): A Widespread Phenomenon in Pharmacological Therapies," Molecules **27**(3), 616 (2022).

[5] T. Kunitake, and S. Shinkai, "Catalysis by Micelles, Membranes and other Aqueous Aggregates as Models of Enzyme Action," edited by V. Gold and D. Bethell, (Academic Press, 1980), pp. 435–487.

[6] A. Naharros-Molinero, M.Á. Caballo-González, F.J. de la Mata, and S. García-Gallego, "Direct and Reverse Pluronic Micelles: Design and Characterization of Promising Drug Delivery Nanosystems," Pharmaceutics **14**(12), 2628 (2022).

[7] M.T. Manzari, Y. Shamay, H. Kiguchi, N. Rosen, M. Scaltriti, and D.A. Heller, "Targeted drug delivery strategies for precision medicines," Nat Rev Mater **6**(4), 351–370 (2021).

[8] C.M. Wells, M. Harris, L. Choi, V.P. Murali, F.D. Guerra, and J.A. Jennings, "Stimuli-Responsive Drug Release from Smart Polymers," J Funct Biomater **10**(3), (2019).

[9] Y. Zhang, W. Song, J. Geng, U. Chitgupi, H. Unsal, J. Federizon, J. Rzayev, D.K. Sukumaran, P. Alexandridis, and J.F. Lovell, "Therapeutic surfactant-stripped frozen micelles," Nat Commun **7**(1), 11649 (2016).

[10] C. Xie, T. Heumüller, W. Gruber, X. Tang, A. Classen, I. Schuldes, M. Bidwell, A. Späth, R.H. Fink, T. Unruh, I. McCulloch, N. Li, and C.J. Brabec, "Overcoming efficiency and stability limits in water-processing nanoparticular organic photovoltaics by minimizing microstructure defects," Nat Commun **9**(1), 5335 (2018).

[11] S. Tiwari, V. Kansara, and P. Bahadur, "Targeting anticancer drugs with pluronic aggregates: Recent updates," Int J Pharm **586**, (2020).

[12] A. Pitto-Barry, and N.P.E. Barry, "Pluronic® block-copolymers in medicine: from chemical and biological versatility to rationalisation and clinical advances," Polym. Chem. **5**(10), 3291–3297 (2014).

[13] S.-Y. Wang, H.-Z. Hu, X.-C. Qing, Z.-C. Zhang, and Z.-W. Shao, "Recent advances of drug delivery nanocarriers in osteosarcoma treatment," J Cancer **11**(1), 69–82 (2020).

[14] A.M. Gerardos, A. Balafouti, and S. Pispas, "Mixed Copolymer Micelles for Nanomedicine," Nanomanufacturing **3**(2), 233–247 (2023).

[15] C. Xu, J. Xu, Y. Zheng, Q. Fang, X. Lv, X. Wang, and R. Tang, "Active-targeting and acid-sensitive pluronic prodrug micelles for efficiently overcoming MDR in breast cancer," J. Mater. Chem. B **8**(13), 2726–2737 (2020).

[16] G. Pérez-Sánchez, F.A. Vicente, N. Schaeffer, I.S. Cardoso, S.P.M. Ventura, M. Jorge, and J.A.P. Coutinho, "Rationalizing the Phase Behavior of Triblock Copolymers through Experiments and Molecular Simulations," The Journal of Physical Chemistry C **123**(34), 21224–21236 (2019).

[17] D. Patel, G. Pérez-Sánchez, M. Jorge, D. Ray, V.K. Aswal, K. Kuperkar, J.A.P. Coutinho, and P. Bahadur, "Rationalizing the Design of Pluronics–Surfactant Mixed Micelles through Molecular Simulations and Experiments," Langmuir **39**(7), 2692–2709 (2023).

[18] G. Pérez-Sánchez, F.A. Vicente, N. Schaeffer, I.S. Cardoso, S.P.M. Ventura, M. Jorge, and J.A.P. Coutinho, "Unravelling the Interactions between Surface-Active Ionic Liquids and Triblock Copolymers for the Design of Thermal Responsive Systems," J Phys Chem B **124**(32), 7046–7058 (2020).

[19] W. Lin, Z. Xue, L. Wen, Y. Li, Z. Liang, J. Xu, C. Yang, Y. Gu, J. Zhang, X. Zu, H. Luo, G. Yi, and L. Zhang, "Mesoscopic simulations of drug-loaded diselenide crosslinked micelles: Stability, drug loading and release properties," Colloids Surf B Biointerfaces **182**, 110313 (2019).

[20] A. Benko, "Nanocarrier drug resistant tumor interactions: novel approaches to fight drug resistance in cancer," Cancer Drug Resistance, (2020).

[21] P. Katiyar, and J.K. Singh, "A coarse-grain molecular dynamics study of oil-water interfaces in the presence of silica nanoparticles and nonionic surfactants," Journal of Chemical Physics **146**(20), (2017).

[22] R. Alessandri, F. Grünewald, and S.J. Marrink, "The Martini Model in Materials Science," Advanced Materials **33**(24), (2021).

[23] G. Pérez-Sánchez, N. Schaeffer, A.M. Lopes, J.F.B. Pereira, and J.A.P. Coutinho, "Using coarse-grained molecular dynamics to understand the effect of ionic liquids on the aggregation of Pluronic copolymer solutions," Physical Chemistry Chemical Physics **23**(10), 5824–5833 (2021).

[24] H. Bastos, R. Bento, N. Schaeffer, J.A.P. Coutinho, and G. Pérez-Sánchez, "Using coarse-grained molecular dynamics to rationalize biomolecule solubilization mechanisms in ionic liquid-based colloidal systems," Physical Chemistry Chemical Physics **22**(42), 24771–24783 (2020).

[25] D. Bedrov, C. Ayyagari, and G.D. Smith, "Multiscale Modeling of Poly(ethylene oxide)−Poly(propylene oxide)−Poly(ethylene oxide) Triblock Copolymer Micelles in Aqueous Solution," J Chem Theory Comput **2**(3), 598–606 (2006).

[26] B. Raubenolt, G. Gyawali, W. Tang, K. Wong, and S. Rick, "Coarse-Grained Simulations of Aqueous Thermoresponsive Polyethers," Polymers (Basel) **10**(5), 475 (2018).

[27] R. Chudoba, J. Heyda, and J. Dzubiella, "Temperature-Dependent Implicit-Solvent Model of Polyethylene Glycol in Aqueous Solution," J Chem Theory Comput **13**(12), 6317–6327 (2017).

[28] R.M. Ziolek, J. Omar, W. Hu, L. Porcar, G. González-Gaitano, C.A. Dreiss, and C.D. Lorenz, "Understanding the pH-Directed Self-Assembly of a Four-Arm Block Copolymer," Macromolecules **53**(24), 11065–11076 (2020).

[29] R.M. Ziolek, P. Smith, D.L. Pink, C.A. Dreiss, and C.D. Lorenz, "Unsupervised Learning Unravels the Structure of Four-Arm and Linear Block Copolymer Micelles," Macromolecules **54**(8), 3755–3768 (2021).

[30] M. Abraham, A. Alekseenko, C. Bergh, C. Blau, E. Briand, M. Doijade, S. Fleischmann, V. Gapsys, G. Garg, S. Gorelov, G. Gouaillardet, A. Gray, M.E. Irrgang, F. Jalalypour, J. Jordan, C. Junghans, P. Kanduri, S. Keller, C. Kutzner, J.A. Lemkul, M. Lundborg, P. Merz, V. Miletić, D. Morozov, S. Páll, R. Schulz, M. Shirts, A. Shvetsov, B. Soproni, D. van der Spoel, P. Turner, C. Uphoff, A. Villa, S. Wingbermühle, A. Zhmurov, P. Bauer, B. Hess, and E. Lindahl, "GROMACS 2023 Source code," (2023).

[31] R.W. Hockney, S.P. Goel, and J.W. Eastwood, "Quiet high-resolution computer models of a plasma," J Comput Phys **14**(2), 148–158 (1974).

[32] T. Darden, D. York, and L. Pedersen, "Particle mesh Ewald: An N·log(N) method for Ewald sums in large systems," J Chem Phys **98**(12), 10089–10092 (1993).

[33] B. Hess, H. Bekker, H.J.C. Berendsen, and J.G.E.M. Fraaije, "LINCS: A linear constraint solver for molecular simulations," J Comput Chem **18**(12), 1463–1472 (1997).

[34] G. Bussi, D. Donadio, and M. Parrinello, "Canonical sampling through velocity rescaling," J Chem Phys **126**(1), 014101 (2007).

[35] M. Parrinello, and A. Rahman, "Polymorphic transitions in single crystals: A new molecular dynamics method," J Appl Phys **52**(12), 7182–7190 (1981).

[36] T. Zhong, P. Ai, and J. Zhou, "Structures and properties of PAMAM dendrimer: A multi-scale simulation study," Fluid Phase Equilib **302**(1–2), 43–47 (2011).

[37] G. Pérez-Sánchez, F.A. Vicente, N. Schaeffer, I.S. Cardoso, S.P.M. Ventura, M. Jorge, and J.A.P. Coutinho, "Rationalizing the Phase Behavior of Triblock Copolymers through Experiments and Molecular Simulations," The Journal of Physical Chemistry C **123**(34), 21224–21236 (2019).

[38] L. Zhao, M. Ren, Y. Wang, H. An, and F. Sun, "Delivery mechanism of doxorubicin by PEG–DPPE micelles on membrane invasion by dynamic simulations," Physical Chemistry Chemical Physics **25**(23), 16114–16125 (2023).

[39] P. Gao, J. Nicolas, and T. Ha-Duong, "Supramolecular Organization of Polymer Prodrug Nanoparticles Revealed by Coarse-Grained Simulations," J Am Chem Soc **143**(42), 17412–17423 (2021).

[40] N. Castillo, L. Monticelli, J. Barnoud, and D.P. Tieleman, "Free energy of WALP23 dimer association in DMPC, DPPC, and DOPC bilayers," Chem Phys Lipids **169**, 95–105 (2013).

[41] L. Martínez, R. Andrade, E.G. Birgin, and J.M. Martínez, "PACKMOL: A package for building initial configurations for molecular dynamics simulations," J Comput Chem **30**(13), 2157–2164 (2009).

[42] W. Humphrey, A. Dalke, and K. Schulten, "VMD: Visual molecular dynamics," J Mol Graph **14**(1), 33–38 (1996).

[43] T.A. Wassenaar, H.I. Ingólfsson, R.A. Böckmann, D.P. Tieleman, and S.J. Marrink, "Computational Lipidomics with *insane* : A Versatile Tool for Generating Custom Membranes for Molecular Simulations," J Chem Theory Comput **11**(5), 2144–2155 (2015).

[44] R. Guixà-González, I. Rodriguez-Espigares, J.M. Ramírez-Anguita, P. Carrió-Gaspar, H. Martinez-Seara, T. Giorgino, and J. Selent, "MEMBPLUGIN: studying membrane complexity in VMD," Bioinformatics **30**(10), 1478–1480 (2014).

[45] D. Drabik, G. Chodaczek, S. Kraszewski, and M. Langner, "Mechanical Properties Determination of DMPC, DPPC, DSPC, and HSPC Solid-Ordered Bilayers," Langmuir **36**(14), 3826–3835 (2020).

[46] D. Poger, B. Caron, and A.E. Mark, "Validating lipid force fields against experimental data: Progress, challenges and perspectives," Biochimica et Biophysica Acta (BBA) - Biomembranes **1858**(7), 1556–1565 (2016).

[47] C.J. Dickson, R.C. Walker, and I.R. Gould, "Lipid21: Complex Lipid Membrane Simulations with AMBER," J Chem Theory Comput **18**(3), 1726–1736 (2022).

[48] N. Agrawal, and E. Parisini, "Investigating the Effects of the POPC–POPG Lipid Bilayer Composition on PAP248–286 Binding Using CG Molecular Dynamics Simulations," J Phys Chem B **127**(42), 9095–9101 (2023).

[49] T.S. Banipal, and A.K. Sood, "Effect of Hydrophobicity and Temperature on the Interactions in the Mixed Micelles of Triblock Polymers [(EO_{76} PO_{29} EO_{76}) and (EO_{19} PO_{69} EO_{19})] with Monomeric and Gemini Surfactants," J Surfactants Deterg **17**(6), 1169–1180 (2014).

[50] P. Singla, O. Singh, S. Sharma, K. Betlem, V.K. Aswal, M. Peeters, and R.K. Mahajan, "Temperature-Dependent Solubilization of the Hydrophobic Antiepileptic Drug Lamotrigine in Different Pluronic Micelles—A Spectroscopic, Heat Transfer Method, Small-Angle Neutron Scattering, Dynamic Light Scattering, and in Vitro Release Study," ACS Omega **4**(6), 11251–11262 (2019).

[51] G. Wanka, H. Hoffmann, and W. Ulbricht, "Phase Diagrams and Aggregation Behavior of Poly(oxyethylene)-Poly(oxypropylene)-Poly(oxyethylene) Triblock Copolymers in Aqueous Solutions," Macromolecules **27**(15), 4145–4159 (1994).

[52] H. Han, S. Li, Y. Zhong, Y. Huang, K. Wang, Q. Jin, J. Ji, and K. Yao, "Emerging pro-drug and nano-drug strategies for gemcitabine-based cancer therapy," Asian J Pharm Sci **17**(1), 35–52 (2022).

[53] A. Dickey, and R. Faller, "Examining the Contributions of Lipid Shape and Headgroup Charge on Bilayer Behavior," Biophys J **95**(6), 2636–2646 (2008).

[54] H.A. Faizi, S.L. Frey, J. Steinkühler, R. Dimova, and P.M. Vlahovska, "Bending rigidity of charged lipid bilayer membranes," Soft Matter **15**(29), 6006–6013 (2019).

[55] H. Kim, B. Fábián, and G. Hummer, "Neighbor List Artifacts in Molecular Dynamics Simulations," J Chem Theory Comput **19**(23), 8919–8929 (2023).

[56] L.R. Cambrea, and J.S. Hovis, "Formation of Three-Dimensional Structures in Supported Lipid Bilayers," Biophys J **92**(10), 3587–3594 (2007).

[57] N.U. Khaliq, J. Lee, S. Kim, D. Sung, and H. Kim, "Pluronic F-68 and F-127 Based Nanomedicines for Advancing Combination Cancer Therapy," Pharmaceutics **15**(8), 2102 (2023).